Molten-salt thermosynthesis of amorphous RuCoFe nanosheets as bifunctional catalysts for electrochemical water splitting

Jiaxi Zhang[1] · Zebi Zhao[1] · Ruyue Wang[1] · Peng Du[1] · Xian He[1] · Xinlai Zhang[1] · Jingkai Yang[1] · Wenjun Liu[1] · Kai Huang[1] · Xuchao Pan[2] · Ming Lei[1]

Abstract

Efficient electrolysis of water is vital to realize the sustainable development of energy, but it is still a challenge. Herein, we propose a common approach to prepare amorphous noble metal alloy nanosheets as advanced bifunctional catalysts to drive the efficient electrochemical water splitting by rapidly annealing metal acetylacetonate (metal = Ru,Co,Fe) and alkali salts, which allows to optimize their catalytic properties by tuning the introduction of transition metals. In particular, as-prepared amorphous RuCoFe nanosheets achieve not only an extremely low overpotential of 2.04 mV at 10 mA cm^{-2} for hydrogen evolution reaction under alkaline media, but also a high-performance and stable overall water electrolysis with a potential of mere 1.56 V at 10 mA cm^{-2}. Considering the advantages of polymetallic amorphous nanosheets electrocatalysts, our proposed synthetic strategy could be versatile and applicable toward further developing other functional polycompounds for energy generation, storage and conversion.

Keywords Rapid annealing · Amorphous nanosheets · Water splitting · Electrocatalysis

1 Introduction

To develop, the energy conversion based on "electrochemical water cycle" is a significant way to realizing a green energy future, where the electrolyzed water is converted into hydrogen and supplied to the fuel cell to generate electricity [1]. At present, the overall electrochemical water splitting (EWS) including hydrogen evolution reaction (HER) and oxygen evolution reaction (OER) can efficiently produce a large amount of hydrogen [2, 3]. Generally speaking, the OER process requires a larger overpotential than HER, so

the actual efficiency of traditional EWS devices will be constrained by the slow OER process [4]. Effective electrocatalysts, Pt/C for HER and Ru-based and Ir-based oxides for OER at this stage, are inevitably exploited and adopted to actuate EWS devices [5]. However, due to the expensive cost and limited storage on earth of noble metals, their large-scale use is greatly restricted. In addition, none of these catalysts can show outstanding performance for both HER and OER simultaneously, which leads to a complicated catalyst preparation process and further increases commercial costs [6–8]. Therefore, it is significant to explore high-efficiency bifunctional catalysts with low usage of noble metal toward HER and OER for overall electrochemical water splitting [9, 10].

Over the years, countless experiments and theories have proved that RuO$_2$ is an excellent OER catalyst, and some papers have also been published that metal Ru has superior HER catalytic activity compared to Pt in an alkaline solution [11–14]. Considering the inexpensive essence of Ru relative to Pt, Ru element-based catalysts may play an important role in alkaline water electrolysis [15]. Recently, Ru-based alloy nanomaterials have been considered as highly active catalysts. For instance, by encapsulating a bimetallic nano-alloy of ruthenium and cobalt in a nitrogen-doped

✉ Kai Huang
huang-kai@bupt.edu.cn

✉ Xuchao Pan
pxchxc@njust.edu.cn

✉ Ming Lei
mlei@bupt.edu.cn

[1] State Key Laboratory of Information Photonics and Optical Communications &, School of Science, Beijing University of Posts and Telecommunications, Beijing 100876, People's Republic of China

[2] Ministerial Key Laboratory of ZNDY, Nanjing University of Science &Technology, Nanjing 210094, China

graphene layer to enhance the carbon–hydrogen bond, it not only reduces the usage of noble metal but also enhances the HER activity [16]. Moreover, compared with crystalline materials, amorphous materials have a large number of randomly oriented bonds, and consequently, their surface has a large quantity of defects and coordination unsaturated sites to improve catalytic performance [17]. For example, in the alkaline electrolyte, the amorphous FeCoW oxyhydroxide has more remarkable OER performance than its crystal [18]. Nevertheless, noble metal nanomaterials prepared by conventional methods are usually crystals with relatively large sizes. Consequently, it is of great significance to synthesize amorphous noble metal alloy catalysts, while the problems faced are quite tricky.

In terms of morphology, two-dimensional (2D) morphology has a larger surface, which can expose more atoms as active sites, thereby enhancing electrochemical performance [19, 20]. In this paper, we propose a rapid heating strategy to synthesize amorphous noble metal Ru-based nanosheets (NSs), such as Ru NSs, RuCo NSs, RuFe NSs and RuCoFe NSs. Due to the strong synergy effect between metals, RuCoFe NSs have the best catalytic performance. Electrochemical tests have proven that under alkaline conditions, RuCoFe NSs show excellent bifunctional catalytic performance for OER and HER in a series of samples, with low overpotentials of 180 mV and 2.04 mV to achieve current density of 10 mA cm^{-2}, which is more prominent than that of commercially available catalysts (Pt/C and IrO$_2$). Significantly, the obtained RuCoFe NSs catalyst displays the greatest activity toward overall water splitting, achieving an applied potential of 1.56 V under the same current density conditions in 1.0 M KOH. In general, this work not only provides a conventional strategy that can effectively prepare 2D amorphous nanomaterials, but also allows a potential stable modification via variety of metal or nonmetal elements to further improve their electrochemical performance for applications.

2 Experimental Part

Ru NSs, RuCo NSs, RuFe NSs and RuCoFe NSs are prepared by mixing acetylacetone metal salt (Metal = Ru,Co,Fe) and alkali metal salt (KBr). In addition, we have also tested the morphology, chemical composition and electrochemical performance of these samples. For specific experimental details, please refer to the supplementary information.

3 Results and Discussion

Figure 1 shows a common and convenient process for preparing amorphous noble metal nanosheets. By replacing or mixing different acetylacetonates, a series of alloy nanosheets are obtained (Ru NSs, RuCo NSs and RuFe NSs, RuCoFe NSs). Typical transmission electron microscopy (TEM) image demonstrates the typical two-dimensional morphology of NSs with the lateral size up to a few micrometers (Fig. S1-S3 and Fig. 2a). In Fig. 2b, the aberration-corrected high-angle annular dark-field scanning TEM (HAADF-STEM) image displays an irregular atomic structure, confirming not a crystal state, which meets the result of diffraction halo-like selected area electron diffraction (SAED) mode (the inset in Fig. 2b). Moreover, the homogeneous distribution of RuCoFe NSs has also been revealed by the energy dispersive spectroscopy (EDS) elemental mapping of Ru, Co, Fe, C and O elements (Fig. 2czh). In addition, a series of samples were subjected to X-ray diffraction (XRD). As shown in Fig. 3a, the spectral line shapes of the four samples are basically similar, and no obvious characteristic peaks can be detected. These results indicate that a variety of samples prepared by the rapid heating method have typical amorphous structures.

Furthermore, in order to determine the chemical composition and coordination environment of the samples, we also performed X-ray photoelectron spectroscopy (XPS) characterization. Here, the Ru *3p* spectrum is used to analyze


Fig. 1 A brief synthesis diagram of amorphous noble metal alloy NSS
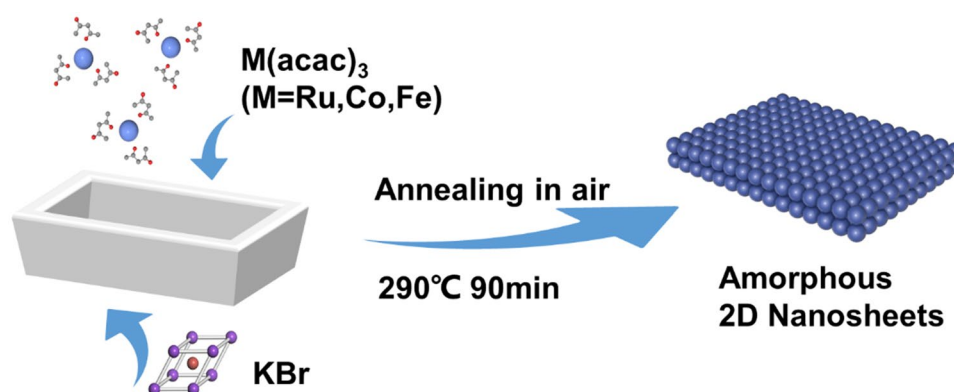
Fig. 2 Morphology characterizations of amorphous RuCoFe nanosheets. **a** TEM, **b** aberration-corrected HAADF-STEM image. The illustration in (**b**) shows the SAED pattern. **c-h** HAADF-STEM image and EDS elemental mapping
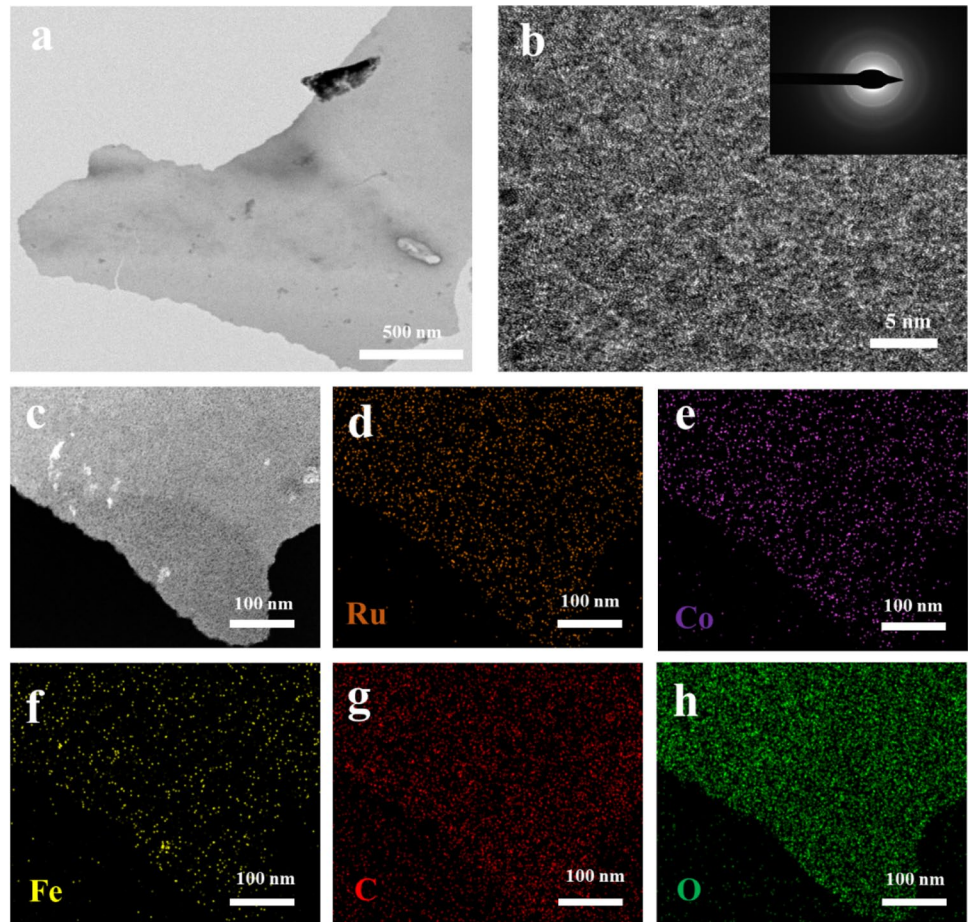
Fig. 3 Structural and compositional characterization of RuCoFe NSs and other samples. **a** XRD patterns. **b-d** XPS spectra of Ru 3p, Co 2p and Fe 2p
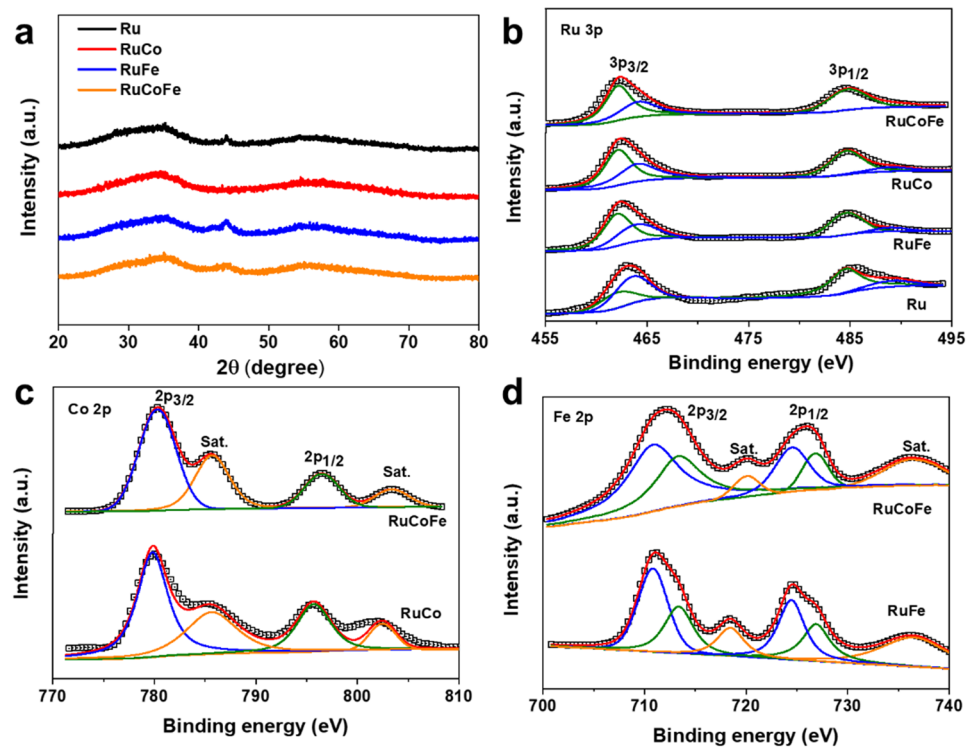
ruthenium to avoid the interference of the carbon substrate. It can be seen from Fig. 3b that the Ru 3p spectrum has two spin–orbital splits, which are Ru $3p_{3/2}$ and Ru $3p_{1/2}$, and the Ru $3p_{3/2}$ peak can be fitted to the metallic Ru^0 (462.1 eV) [21] and Ru^{4+} (464.1 eV) peaks [22], the Ru $3p_{1/2}$ peak can be fitted to the metallic Ru^0 (484.7 eV) and Ru^{4+} (489.4 eV) peaks [23], which have been demonstrated to be a catalytic active site [24]. We can clearly see that compared with Ru NSs, RuCo NSs, RuFe NSs, the Ru 3p spectrum of the RuCoFe NSs shows a positive shift, indicating that the electron density of Ru is low. The Co $2p$ spectra indicate that the fitted peaks at 779.7 eV and 794.6 eV are assigned to Co^{3+}, and the fitted peaks at 781.4 eV and 796.5 eV are ascribed to Co^{2+} (Fig. 3(c)) [25]. It is well known that Co^{2+} oxide can greatly promote the water decomposition step involved in alkaline for HER [26]. In addition, since Co^{2+} is partially oxidized to Co^{3+} ions, this may promote the charge transfer in the electrochemical process. By using the Gaussian fitting method, the Fe $2p$ spectrum is well deconvolved into two spin–orbit doublets and two other satellites in Fig. 3d, the fitting peaks at of 711.8 eV and 724.5 eV are assigned to the Fe^{2+}, while the fitting peaks at 713.3 eV and 726.8 eV are ascribed to the Fe^{3+} [27]. Similarly, compared with the other three samples, Co 2p spectra and Fe 2p spectra of RuCoFe all showed a positive shift which performed that there may be a powerful electronic interaction between the RuCoFe alloy nanosheets. The higher the binding energy of Co and Fe elements, the higher the possibility of the resulting oxidation state, which is more conducive to the catalytic activity of OER. [28–32]. Furthermore, we performed TEM characterization of RuCoFe NSs after stability test, and after comparison, it can be seen that the morphology of RuCoFe NSs has not changed significantly (Fig. S4). In addition, it can be seen from Fig. S5 that compared with Fig. 3, the XPS spectrum of RuCoFe NSs obtained after the stability test has negligible changes, which indicates that there is almost no change in the valence state of the element during the electrocatalysis process. The above results all prove that RuCoFe NSs have excellent stability in alkaline environment.

For electrochemical testing, we use a three-electrode electrochemical system to test the OER and HER performance of the synthesized samples in 1 M KOH. In order to avoid the negative influence of ohmic resistance on the measured anode current, iR correction was applied to all initial data to further analyze intrinsic activity. As shown in Fig. 4a, in the case of a current density of 10 mA cm^{-2}, the RuCoFe NSs have an overpotential of 180 mV, which is much better than the other four samples including the Ru NSs (250 mV), RuCo NSs (210 mV), RuFe NSs (220 mV) and commercial catalyst IrO_2 (350 mV). Besides, the prominent OER performance of RuCoFe NSs was proved by the smallest Tafel slopes derived from LSVs (69.18 mV dec^{-1}, Fig. 4b), compared with Ru NSs (167.49 mV dec^{-1}), RuCo

NSs (75.66 mV dec^{-1}), RuFe NSs (184.77 mV dec^{-1}) and IrO_2 (177.58 mV dec^{-1}). Impressively, the OER activity of the RuCoFe NSs performed wonderful performance in the recently reported articles (Table S1). Besides activity, another vital property for evaluating the performance of OER electrocatalysts is stability. Unexpectedly, even after 5000 cycles, the OER activity of RuCoFe NSs has not changed much (Fig. 4c). In addition, Fig. S6 further tests the long-term electrochemical catalytic stability of RuCoFe NSs to OER through a typical chronoamperometry (CA). After 10 h of testing, the current density of RuCoFe NSs remained at 90% of the initial current density.

Furthermore, the RuCoFe NSs electrode also has high activity for the cathodic process of water splitting. Compared with other samples including the Ru NSs (41.53 mV), RuCo NSs (16.89 mV), RuFe NSs (30.33 mV) and commercial catalyst Pt/C (10.16 mV), the minimum overpotential of RuCoFe NSs is 2.04 mV for HER when the current density is the same as that of OER (Fig. 4d). The Tafel plots in Fig. 4e provide a further mechanism analysis of the catalytic reaction kinetics. The Tafel slope of RuCoFe NSs is estimated to be 33.07 mV dec^{-1}, more excellent than these of Ru NSs (115.31 mV dec^{-1}), RuCo NSs (91.99 mV dec^{-1}), RuFe NSs (92.95 mV dec^{-1}) and Pt/C (72.99 mV dec^{-1}). It is noteworthy that the HER activity of the RuCoFe NSs also proved outstanding performance in the recently reported high-efficiency HER electrocatalysts (Table S2). At the same time, the 5000-cycles ADT test performed by cyclic voltammetry and the typical chronoamperometry (CA) in Fig. 4f and Fig. S7 also showed excellent stability under HER conditions. Besides, the Nyquist plots (Fig. S8-S9) indicated that compared with all tested catalysts, RuCoFe NSs have the lowest charge transfer resistance, which proved that the charge transfer process of RuCoFe NSs was faster. As for the total water splitting, we constructed a two-electrode system using two identical RuCoFe NSs at the anode and cathode (Fig. S10). The illustration in Fig. 4g shows that when the voltage is 1.6 V, a large amount of hydrogen overflows at the cathode of the electrode, and a large amount of oxygen overflows on the other side of the electrode. The two-electrode device has excellent catalytic performance and only requires a voltage of 1.56 V to achieve a current density of 10 mA cm^{-2}, please note that commercial electrodes (Pt/C and IrO_2) are 40 mV higher than it. The Tafel slope of RuCoFe NSs (256 mV dec^{-1}) is also smaller than that of the commercial electrodes system (267 mV dec^{-1}, Fig. S11). It is impressive that RuCoFe NSs are one of the catalysts with high total water splitting activity among most electrocatalysts reported recently (Table S3). Furthermore, Fig. 4h shows that the device lasted for 10 h at 1.56 V in the CA test, showing unparalleled stability. After this test, the almost unchanged LSV (Fig. 4i) further supports the stability of the overall hydrolysis. All the data prove that RuCoFe
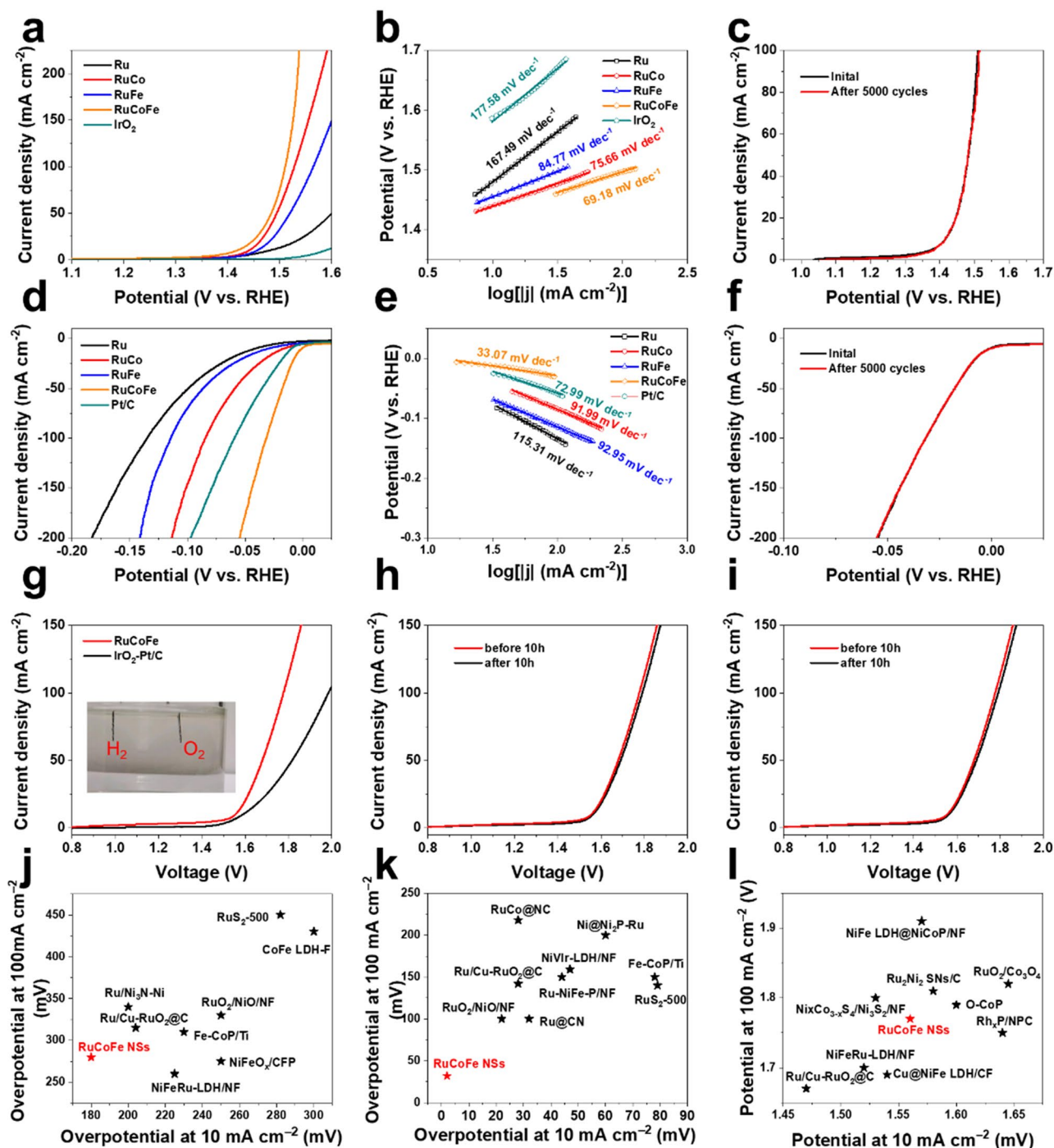
Fig. 4 Electrocatalytic properties for OER, HER and EWS in 1 M KOH. **a** OER LSV curves and **b** Tafel plots. **c** ADT for OER **d** HER LSV curves and **e** Tafel plots. **f** ADT for HER. **g** LSV curves of EWS devices. **h** LSV curves of the EWS device before and after 10 h CA test. **i** Chronoamperometric response curves of the EWS device. **j-l** Comparison of the overpotential of RuCoFe in 1.0 M KOH with other noble metals or Co/Fe-based catalysts

NSs have excellent OER and HER performance (Fig. 4j-l), which is probably due to the amorphous structure of RuCoFe NSs and the synergy between the three elements of Ru, Co and Fe, thereby increasing abundant active sites and improving reaction kinetics.

4 Conclusions

We demonstrated a general and effective method for synthesizing the amorphous noble metal alloy nanosheets by rapidly annealing the mixture of metal acetylacetonate and

alkali salts. As a bifunctional catalyst, RuCoFe NSs showed the superexcellent OER and HER performance and stability in an alkaline solution. Particularly, for OER, it only needs 180 mV of overpotential to reach 10 mA cm^{-2}, and HER only needs 2.04 mV. Beyond the modulation toward nanocatalysts, we believe the proposed strategy will innovate new inspirations for pursuing 2D nanostructure with desired surface structure and composition to extend the potential applications in various fields.

References

1. Z.W. Zhuang, Y. Wang, C.Q. Xu, S.J. Liu, C. Chen, Q. Peng, Z.B. Zhuang, H. Xiao, Y. Pan, S.Q. Lu, R. Yu, W.C. Cheong, X. Cao, K.L. Wu, K.A. Sun, Y. Wang, D.S. Wang, J. Li, Y.D. Li, Three-dimensional open nano-netcage electrocatalysts for efficient pH-universal overall water splitting. Nat. Commun. **10**, 4875 (2019)

2. D. Chen, R.H. Lu, Z.H. Pu, J.W. Zhu, H.W. Li, F. Liu, S. Hu, X. Luo, J.S. Wu, Y. Zhao, S.C. Mu, Ru-doped 3D flower-like bimetallic phosphide with a climbing effect on overall water splitting, Appl. Catal. B-Environ. **279**, 119396 (2020).

3. W. Liu, L. Pang, H. Han, K. Bi, M. Lei, Z. Wei, Tungsten disulphide for ultrashort pulse generation in all-fiber lasers. Nanoscale **9**, 5806–5811 (2017)

4. Y. Jiao, Y. Zheng, M. Jaroniec, S.Z. Qiao, Design of electrocatalysts for oxygen- and hydrogen-involving energy conversion reactions. Chem. Soc. Rev. **44**, 2060–2086 (2015)

5. L. Zhao, Y. Zhang, Z.L. Zhao, Q.H. Zhang, L.B. Huang, L. Gu, G. Lu, J.S. Hu, L.J. Wan, Steering elementary steps towards efficient alkaline hydrogen evolution via size-dependent Ni/NiO nanoscale heterosurfaces. Natl. Sci. Rev. **7**, 27–36 (2020)

6. T. He, Y. Peng, Q.X. Li, J.E. Lu, Q.M. Liu, R. Mercado, Y. Chen, F. Nichols, Y. Zhang, S.W. Chen, Nanocomposites based on ruthenium nanoparticles supported on cobalt and nitrogen-codoped graphene nanosheets as bifunctional catalysts for electrochemical water splitting. ACS Appl. Mater. Interfaces. **11**, 46912–46919 (2019)

7. K. Huang, R.Y. Wang, S.J. Zhao, P. Du, H. Wang, H.H. Wei, Y.Z. Long, B.H. Deng, M. Lei, B.H. Ge, H.Y. Gou, R. Zhang, H. Wu, Atomic species derived CoO$_x$ clusters on nitrogen doped mesoporous carbon as advanced bifunctional electro-catalysts for Zn-air battery. Energy Storage Mater. **29**, 156–162 (2020)

8. E.M. Miner, T. Fukushima, D. Sheberla, L. Sun, Y. Surendranath, M. Dincă, Electrochemical oxygen reduction catalysed by Ni$_3$(hexaiminotriphenylene)$_2$. Nat. Commun. **7**, 10942 (2016)

9. K. Huang, S. Guo, R.Y. Wang, S. Lin, N. Hussain, H.H. Wei, B.H. Deng, Y.Z. Long, M. Lei, H.L. Tang, H. Wu, Two-dimensional MOF/MOF derivative arrays on nickel foam as efficient bifunctional coupled oxygen electrodes. Chin. J. Catal. **41**, 1754–1760 (2020)

10. W.J. Liu, L.H. Pang, H.N. Han, M.L. Liu, M. Lei, S.B. Fang, H. Teng, Z.Y. Wei, Tungsten disulfide saturable absorbers for 67 fs mode-locked erbium-doped fiber lasers. Opt. Express. **25**, 2950–2959 (2017)

11. E. Yilmaz, C. Yogi, K. Yamanaka, T. Ohta, H.R. Byon, Promoting formation of noncrystalline Li$_2$O$_2$ in the Li–O$_2$ battery with RuO$_2$ nanoparticles. Nano Lett. **13**, 4679–4684 (2013)

12. R.R. Rao, M.J. Kolb, N.B. Halck, A.F. Pedersen, A. Mehta, H. You, K.A. Stoerzinger, Z.X. Feng, H.A. Hansen, H. Zhou, L. Giordano, J. Rossmeisl, T. Vegge, I. Chorkendorff, I.E.L. Stephens, Y.S. Horn, Towards identifying the active sites on RuO$_2$(110) in catalyzing oxygen evolution. Energy Environ. Sci. **10**, 2626–2637 (2017)

13. K. Huang, Z.B. Zhao, H.F. Du, P. Du, H. Wang, R.Y. Wang, S. Lin, H.H. Wei, Y.Z. Long, M. Lei, W. Guo, H. Wu, Rapid thermal annealing toward high-quality 2D cobalt fluoride oxide as an advanced oxygen evolution electrocatalyst. ACS Sustainable Chem. Eng. **8**, 6905–6913 (2020)

14. Y. Zheng, Y. Jiao, Y.H. Zhu, L.H. Li, Y. Han, Y. Chen, M. Jaroniec, S.Z. Qiao, High electrocatalytic hydrogen evolution activity of an anomalous ruthenium catalyst. J. Am. Chem. Soc. **138**, 16174–16181 (2016)

15. Z. Liu, M. Zha, Q. Wang, G.Z. Hu, L.G. Feng, Overall water-splitting reaction efficiently catalyzed by a novel bi-functional Ru/Ni$_3$N-Ni electrode. Chem. Commun. **56**, 2352–2355 (2020)

16. J.W. Su, Y. Yang, G.L. Xia, J.T. Chen, P. Jiang, Q.W. Chen, Ruthenium-cobalt nanoalloys encapsulated in nitrogen-doped graphene as active electrocatalysts for producing hydrogen in alkaline media. Nat. Commun. **8**, 14969 (2017)

17. G. Wu, X.S. Zheng, P.X. Cui, H.Y. Jiang, X.Q. Wang, Y.T. Qu, W.X. Chen, Y. Lin, H. Li, X. Han, Y.M. Hu, P.G. Liu, Q.H. Zhang, J.J. Ge, Y.C. Yao, R.B. Sun, Y.E. Wu, L. Gu, X. Hong, Y.D. Li, A general synthesis approach for amorphous noble metal nanosheets. Nat. Commun. **10**, 4855 (2019)

18. B. Zhang, X.L. Zheng, O. Voznyy, R. Comin, M. Bajdich, M. García-Melchor, L.L. Han, J.X. Xu, M. Liu, L.R. Zheng, F.P. García de Arquer, C.T. Dinh, F.J. Fan, M.J. Yuan, E. Yassitepe, N. Chen, T. Regier, P.F. Liu, Y.H. Li, P. De Luna, A. Janmohamed, H.L. Xin, H.G. Yang, A. Vojvodic, E.H. Sargent, Homogeneously dispersed multimetal oxygen-evolving catalysts. Science **352**, 333 (2016)

19. Q. Yao, B.L. Huang, N. Zhang, M.Z. Sun, Q. Shao, X.Q. Huang, Channel-rich RuCu nanosheets for pH-universal overall water splitting electrocatalysis. Angew. Chem.-Int. Edit. **58**, 13983–13988 (2019)

20. W.J. Liu, L.H. Pang, H.N. Han, Z.W. Shen, M. Lei, H. Teng, Z.Y. Wei, Dark solitons in WS$_2$ erbium-doped fiber lasers. Photonics Res. **4**, 111–114 (2016)

21. Z. Liu, X.D. Yang, G.Z. Hu, L.G. Feng, Ru nanoclusters coupled on Co/N-doped carbon nanotubes efficiently catalyzed the hydrogen evolution reaction. ACS Sustain. Chem. Eng. **8**, 9136–9144 (2020)

22. K. Yang, P.P. Xu, Z.Y. Lin, Y. Yang, P. Jiang, C.L. Wang, S. Liu, S.P. Gong, L. Hu, Q.W. Chen, Ultrasmall Ru/Cu-doped RuO$_2$ complex embedded in amorphous carbon skeleton as highly active bifunctional electrocatalysts for overall water splitting. Small **14**, 1803009 (2018)

23. C. Wang, L.M. Qi, Heterostructured inter-doped ruthenium-cobalt oxide hollow nanosheet arrays for highly efficient overall water splitting. Angew. Chem.-Int. Edit. **59**, 17219–17224 (2020)

24. M.I. Qadir, A. Weilhard, J.A. Fernandes, I. de Pedro, B.J.C. Vieira, J.C. Waerenborgh, J. Dupont, Selective carbon dioxide hydrogenation driven by ferromagnetic RuFe banoparticles in ionic liquids. ACS Catal. **8**, 1621–1627 (2018)

25. B. Li, P. Gu, Y.C. Feng, G.X. Zhang, K.S. Huang, H.G. Xue, H. Pang, Ultrathin nickel-cobalt phosphate 2D nanosheets for electrochemical energy storage under aqueous/solid-state electrolyte. Adv. Funct. Mater. **27**, 1605784 (2017)

26. F.F. Zhang, Y.L. Zhu, Y. Chen, Y.Z.H. Lu, Q. Lin, L. Zhang, S.W. Tao, X.W. Zhang, H.T. Wang, RuCo alloy bimodal nanoparticles embedded in N-doped carbon: a superior pH-universal electrocatalyst outperforms benchmark Pt for the hydrogen evolution reaction. J. Mater. Chem. A. **8**, 12810–12820 (2020)

27. M.J. Liu, L.M. Yang, T. Liu, Y.H. Tang, S.L. Luo, C.B. Liu, Y.X. Zeng, Fe_2P/reduced graphene oxide/Fe_2P sandwich-structured nanowall arrays: a high-performance non-noble-metal electrocatalyst for hydrogen evolution. J. Mater. Chem. A. **5**, 8608–8615 (2017)

28. K. Huang, R.Y. Wang, H.B. Wu, H. Wang, X. He, H.H. Wei, S.P. Wang, R. Zhang, M. Lei, W. Guo, B.H. Ge, H. Wu, Direct immobilization of an atomically dispersed Pt catalyst by suppressing heterogeneous nucleation at −40 °C. J. Mater. Chem. A **7**, 25779–25784 (2019)

29. W.J. Liu, Y.N. Zhu, M.L. Liu, B. Wen, S.B. Fang, H. Teng, M. Lei, L.M. Liu, Z.Y. Wei, Optical properties and applications for MoS_2-Sb_2Te_3-MoS_2 heterostructure materials. Photonics Res. **6**, 220–227 (2018)

30. Q.M. Wang, J.M. Zhang, Z.D. Zhang, Y.N. Hao, K. Bi, Enhanced dielectric properties and energy storage density of PVDF nanocomposites by co-loading of $BaTiO_3$ and $CoFe_2O_4$ nanoparticles. Adv. Compos. Hybrid Mater. **3**, 58–65 (2020)

31. J.C. Xu, L.H. Chen, X.J. Zhai, R. Zhang, K.D. Mcdonald-Maier, S.G. Huang, K. Bi, Generation of continuously variable-mode orbital angular momentum beams. Eng. Sci. **10**, 51–57 (2020)

32. Q. Chen, Y. Nie, M. Ming, G.Y. Fan, Y. Zhang, J.S. Hu, Sustainable synthesis of supported metal nanocatalysts for electrochemical hydrogen evolution. Chin J Catal. **41**, 1791–1811 (2020)